

Functional renormalization group study of thermodynamic geometry around the phase transition of quantum chromodynamics

Fabrizio Murgana^{1,2,3}, Vincenzo Greco^{1,4}, Marco Ruggieri^{1,2} and Dario Zappalà^{2,5}

¹*Department of Physics and Astronomy, University of Catania, Via S. Sofia 64, I-95125 Catania, Italy*

²*INFN-Sezione di Catania, Via S. Sofia 64, I-95123 Catania, Italy*

³*Institut für Theoretische Physik, Goethe-Universität, Max-von-Laue-Straße 1, D-60438 Frankfurt am Main, Germany*

⁴*Laboratori Nazionali del Sud, INFN-LNS, Via S. Sofia 62, I-95123 Catania, Italy*

⁵*Centro Siciliano di Fisica Nucleare e Struttura delle Materia, Via S. Sofia 64, I-95123 Catania, Italy*



(Received 7 December 2023; accepted 24 April 2024; published 13 May 2024)

We investigate the thermodynamic geometry of the quark-meson model at finite temperature, T , and quark number chemical potential, μ . We extend previous works by the inclusion of fluctuations exploiting the functional renormalization group approach. We use recent developments to recast the flow equation into the form of an advection-diffusion equation. We adopt the local potential approximation for the effective average action. We focus on the thermodynamic curvature, R , in the (μ, T) plane, in proximity of the chiral crossover, up to the critical point of the phase diagram. We find that the inclusion of fluctuations results in a smoother behavior of R near the chiral crossover. Moreover, for small μ , R remains negative, signaling the fact that bosonic fluctuations reduce the capability of the system to completely overcome the fermionic statistical repulsion of the quarks. We investigate in more detail the small μ region by analyzing a system in which we artificially lower the pion mass, thus approaching the chiral limit in which the crossover is actually a second order phase transition. On the other hand, as μ is increased and the critical point is approached, we find that R is enhanced and a sign change occurs, in agreement with mean field studies. Hence, we completely support the picture that R is sensitive to a crossover and a phase transition, and provides information about the effective behavior of the system at the phase transition.

DOI: [10.1103/PhysRevD.109.096017](https://doi.org/10.1103/PhysRevD.109.096017)

I. INTRODUCTION

Within the theory of fluctuations among equilibrium states, one of the most interesting ideas is given by the thermodynamic curvature [1–26], which represents an innovative perspective in the field of thermodynamics. This employs non-Euclidean geometry to represent fluctuations and interactions among thermodynamic variables. The geometric approach sheds new light on understanding phase transitions and emergent properties in complex systems, providing an intriguing connection between geometry and thermodynamics. In fact, in the grand canonical ensemble one can consider any pair of intensive variables (β^1, β^2) : given these, the probability of a fluctuation from the state $S_1 = (\beta^1, \beta^2)$ to $S_2 = (\beta^1 + \delta\beta^1, \beta^2 + \delta\beta^2)$ is proportional to

$$\sqrt{g} \exp\left(-\frac{d\ell^2}{2}\right). \quad (1)$$

Here,

$$d\ell^2 = g_{\beta^1 \beta^1} d\beta^1 d\beta^1 + 2g_{\beta^1 \beta^2} d\beta^1 d\beta^2 + g_{\beta^2 \beta^2} d\beta^2 d\beta^2, \quad (2)$$

where

$$g_{ij} = \frac{\partial^2 \log \mathcal{Z}}{\partial \beta^i \partial \beta^j} \quad (3)$$

is the metric tensor in the 2-dimensional manifold; \mathcal{Z} is the grand canonical partition function. Finally, g is the determinant of the metric tensor. $d\ell^2$ measures the distance between the states S_1 and S_2 . Equipped with the metric, we introduce the thermodynamic curvature, $R = 2R_{1212}/g$, where R_{1212} corresponds to the only independent component of the Riemann tensor for a two dimensional manifold. R depends on the second and third order moments of the thermodynamic variables that are conjugated to (β^1, β^2) : it thus carries information about the fluctuation of the physical quantities.

Published by the American Physical Society under the terms of the [Creative Commons Attribution 4.0 International license](https://creativecommons.org/licenses/by/4.0/). Further distribution of this work must maintain attribution to the author(s) and the published article's title, journal citation, and DOI. Funded by SCOAP³.

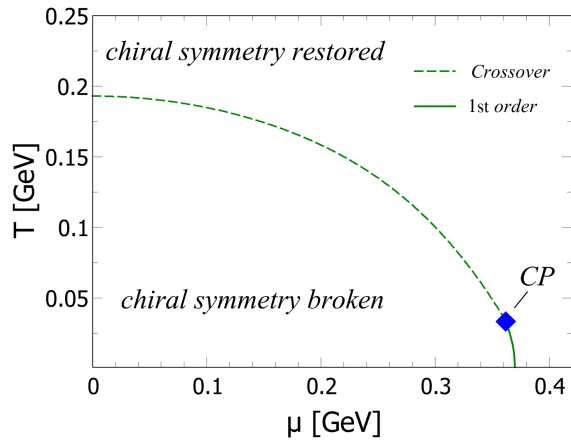


FIG. 1. Phase diagram of the quark-meson model at finite temperature T and chemical potential μ . The chirally spontaneously (and explicitly) broken phase and the (approximately) chirally symmetric phase are indicated in the plot. The dashed line, indicating a crossover, and the 1st order phase transition lines merge at the critical endpoint, labeled CP .

Within the context of thermodynamic geometry, interesting and recent developments regard its applications to effective models, in particular to the quark-meson (QM) model [27,28]. The QM model is a well known low energy effective model of quantum chromodynamics (QCD) [29–32]; it has mostly been used because it could qualitatively capture the chiral phase transition of QCD, i.e., the transition from chiral symmetry broken phase in QCD vacuum, to a chiral symmetry restored phase at finite temperature, T , and quark number chemical potential, μ . In Fig. 1 we show a cartoon phase diagram of the QM model in the (μ, T) plane; the diagram is drawn assuming a finite quark mass which explicitly breaks the chiral symmetry. In the figure, the dashed line corresponds to a smooth crossover, while the solid line to a first order transition; in both cases, chiral symmetry is spontaneously broken in the low temperature phase while it is (approximately) restored in the high temperature phase. The two lines meet at a point, known as the critical endpoint (CP). At this point, the crossover becomes a real second order phase transition with a divergent correlation length. The purpose of the present work is to study the thermodynamic curvature around the crossover, both at small μ and in the proximity of CP .

One of the most viable uses of the QM model is related to the study of the strongly interacting matter at finite T and/or μ . Similarly to the already discussed phase diagram of the QM model, first principle calculations performed in Lattice-QCD (LQCD) [33–35] show that at $\mu = 0$, a smooth crossover happens between a low-temperature phase, in which chiral symmetry is spontaneously broken and the relevant degrees of freedom are hadrons, to a quark-gluon plasma phase at high temperature where chiral symmetry is approximately restored and the relevant degrees of freedom are quarks and gluons. In addition to this, it is commonly

believed that there should exist a critical endpoint in the (T, μ) plane in full QCD, similar to the one found in the QM model, see [36,37] for reviews. However, first principle calculations are not feasible at finite μ due to the (in)famous sign problem [33–35]. This is where effective models, like the QM model, can help.

In this work, we study the QM model at finite T and μ , focusing of its thermodynamic geometry; this is the natural continuation of previous works on the same subject [27,28,38]. The aspect of novelty of the study is the inclusion of the quantum fluctuations via the functional renormalization group approach (FRG) [39–62]; this is based on the ideas introduced by Wilson [44–48] and others, see, e.g., Refs. [49,50]. Since the FRG method belongs to the class of non-perturbative approaches to quantum field theories and it is built in such a way to link different energy scales and the associated degrees of freedom, it is a suitable tool to deal with second order phase transitions and critical long wave length phenomena in general, whose nature is highly nonperturbative.

The reason why the investigation of the critical behavior of the QM model via the thermodynamic geometry is worthy lies in the information one can extract from R on the system. Particularly, it has been argued that the sign of R is connected to the dominance of a fermionic or bosonlike behavior of the system [9,14,15,63]: a positive R corresponds to a bosonlike behavior while a negative R to a fermionlike behavior. This behavior has been understood as attraction or repulsion in the phase space [9,14,15,63]. Therefore, the study of the sign of R near a second order phase transition (and to some extent, around a crossover [27,28,38]) can reveal information about the effective dynamics which develops in the proximity of this transition. Another interesting feature of R , anticipated in [27,28,38], is linked to the presence of a peak structure close to the crossover temperature for small values of μ , which eventually should turn into a divergence when the critical point is reached. We complete the studies of [27,28,38] by analyzing these aspects of R within the FRG approach.

This article is structured as follows: In Sec. II, we briefly introduce the thermodynamic geometry. In Sec. III, we discuss the basic features of the quark-meson model. In Sec. IV, we present a short introduction to the functional renormalization group and how this can be specifically applied to the quark-meson model. In Sec. V, we discuss the results on the thermodynamic geometry for the quark-meson model. Finally, in Sec. VI we draw our conclusions and present an outlook. Within this article we use natural units $\hbar = c = k_B = 1$.

II. THERMODYNAMIC CURVATURE

We consider a thermodynamic system in the grand-canonical ensemble whose equilibrium state is characterized by the pair (μ, T) , where T is the temperature and μ is

the quark number chemical potential (conjugated to quark number density). Thermodynamic geometry is more conveniently defined in terms of the variables $(\beta = 1/T, \gamma = -\mu/T)$. A thermodynamic system at equilibrium at the point (β, γ) can fluctuate to another equilibrium state (β', γ') , and the probability of this fluctuation can be computed within the standard thermodynamic fluctuation theory. In fact, as already mentioned in the introduction, we firstly define a distance in the two-dimensional manifold spanned by (β, γ) ,

$$d\ell^2 = g_{\beta\beta}d\beta d\beta + 2g_{\beta\gamma}d\beta d\gamma + g_{\gamma\gamma}d\gamma d\gamma \quad (4)$$

where the metric tensor is

$$g_{ij} = \frac{\partial^2 \log \mathcal{Z}}{\partial \beta^i \partial \beta^j} = \frac{\partial^2 \phi}{\partial \beta^i \partial \beta^j} \equiv \phi_{,ij}, \quad (5)$$

with $\phi = \beta P$, $P = -\Omega$, and Ω denotes the thermodynamic potential density; moreover, we used the standard notation $\beta^1 = \beta$ and $\beta^2 = \gamma$. Given these, the fluctuation probability is

$$\frac{dp}{d\beta d\gamma} \propto \sqrt{g} \exp\left(-\frac{d\ell^2}{2}\right), \quad (6)$$

where

$$g = g_{\beta\beta}g_{\gamma\gamma} - g_{\beta\gamma}^2 \quad (7)$$

is the determinant of the metric. Large probability of a fluctuation corresponds to small $d\ell^2$. Therefore, a large thermodynamic distance between two equilibrium states means a small probability to fluctuate between the two states. According to these considerations, Eq. (4) measures the distance in the (β, γ) plane between two thermodynamic states in equilibrium.

Thermodynamic stability requires that $g_{\beta\beta} > 0$ and $g > 0$, while $g = 0$ corresponds to a phase boundary and regions with $g < 0$ are thermodynamically unstable: hence, the stability conditions ensure that $d\ell^2 > 0$. Furthermore,

$$V\phi_{,\beta\beta} = \langle (U - \langle U \rangle)^2 \rangle, \quad (8)$$

$$V\phi_{,\beta\gamma} = \langle (U - \langle U \rangle) \rangle \langle (N - \langle N \rangle) \rangle, \quad (9)$$

$$V\phi_{,\gamma\gamma} = \langle (N - \langle N \rangle)^2 \rangle, \quad (10)$$

where U and N denote the internal energy and the particle number, respectively, while V stands for the volume of the system.

Once the manifold has been provided with the metric tensor, one can define the Riemann tensor as

$$R^i_{klm} = \frac{\partial \Gamma^i_{km}}{\partial x^l} - \frac{\partial \Gamma^i_{kl}}{\partial x^m} + \Gamma^i_{nl} \Gamma^n_{km} - \Gamma^i_{nm} \Gamma^n_{kl}, \quad (11)$$

with the Christoffel symbols

$$\Gamma^i_{kl} = \frac{1}{2} g^{im} \left(\frac{\partial g_{mk}}{\partial x^l} + \frac{\partial g_{il}}{\partial x^k} - \frac{\partial g_{kl}}{\partial x^m} \right). \quad (12)$$

The standard contraction procedure gives the Ricci tensor $R_{ij} = R^k_{ikj}$, and the scalar curvature $R = R^i_i$: within thermodynamic geometry, R is called the thermodynamic curvature. For the two-dimensional manifold that we consider in this study the expression of R considerably simplifies, namely [12]

$$R = -\frac{1}{2g^2} \begin{vmatrix} \phi_{,\beta\beta} & \phi_{,\beta\gamma} & \phi_{,\gamma\gamma} \\ \phi_{,\beta\beta\beta} & \phi_{,\beta\beta\gamma} & \phi_{,\beta\gamma\gamma} \\ \phi_{,\beta\beta\gamma} & \phi_{,\beta\gamma\gamma} & \phi_{,\gamma\gamma\gamma} \end{vmatrix}, \quad (13)$$

where $\|$ indicates the determinant of the matrix. The curvature diverges for $g \rightarrow 0$, which corresponds to a phase boundary, unless the numerator of Eq. (13) vanishes on the same boundary.

Let ξ denote the correlation length of the order parameter: then, $|R| \propto \xi^3$ near a second-order phase transition [1], which naturally results from hyperscaling. Theoretical calculations based on different models confirm this hypothesis [1,12,64–66]; therefore, the study of R in the (μ, T) plane allows to estimate the correlation volume based only on the thermodynamic potential: this is one of the merits of the thermodynamic geometry. It has also been suggested that the sign of R conveys details about the nature of the interaction, attractive or repulsive, at a mesoscopic level in proximity of the phase transition.

Within our sign convention, $R > 0$ indicates an attractive interaction while $R < 0$ corresponds to a repulsive one. These interactions include not only real interactions [17,19,24,67,68], but also the statistical attraction and repulsion that ideal quantum gases feel in phase space [69–73]: an ideal fermion gas has $R < 0$ due to the statistical repulsion, while an ideal boson gas has $R > 0$ due to the statistical attraction. The thermodynamic curvature is known to be identically zero only for the ideal classical gas. Other fields of application of thermodynamic geometry include Lennard-Jones fluids [17,67,68], ferromagnetic systems [74], black holes [17,63,75–89], strongly interacting matter [27,90,91], and others [92,93].

III. THE QUARK-MESON MODEL

The quark-meson model (QM) can be understood as arising from the well-known linear-sigma model coupled to fermions ([29–32]). In particular, the $N_f = 2$ QM model uses as fundamental degrees of freedom four mesons, an

isotriplet of pion fields $\vec{\pi} = (\pi^1, \pi^2, \pi^3)$ and an isosinglet field σ , coupled to a massless isodoublet fermionic field ψ representing up and down quarks. The Euclidean Lagrangian density of the model then reads

$$\mathcal{L}_{QM}^E = \bar{\psi}(\gamma_\mu \partial^\mu + h(\sigma + i\gamma^5 \vec{\tau} \vec{\pi}))\psi + \frac{1}{2}(\partial_\mu \sigma)^2 + \frac{1}{2}(\partial_\mu \vec{\pi})^2 + U(\sigma^2 + \vec{\pi}^2) - c\sigma. \quad (14)$$

in which γ_μ and γ^5 are the standard Euclidean Dirac matrices in Dirac space, h is the strength of the Yukawa coupling between quarks and mesons and $\vec{\tau} = (\tau^1, \tau^2, \tau^3)$ represents the vector of Pauli matrices in flavor space. $U(\sigma^2 + \vec{\pi}^2)$ indicates a generic interaction potential among the mesons, and it is constructed in order to be O(4) symmetric, since it depends on the O(4) invariant mesonic combination $\sigma^2 + \vec{\pi}^2$. Anyway, if the potential develops a finite minimum along one radial direction, the O(4) symmetry is spontaneously broken into a O(3) symmetry. Due to this residual symmetry, one is free to choose the ground state in the vacuum as

$$\langle \vec{\pi} \rangle = 0, \quad \langle \sigma \rangle = f_\pi \neq 0, \quad (15)$$

where $f_\pi = 0.093$ GeV is the pion decay constant.

Even though the Lagrangian does not contain an explicit mass term for the fermions, when the symmetry is spontaneously broken they acquire a dynamical constituent mass given by $M = h\langle \sigma \rangle$. Furthermore, the O(4) symmetry is also explicitly broken by the term $-c\sigma$, which mimics the presence of a finite current mass for quarks. In this way, the pions turn into massive pseudo-Goldstone mesons, since the spontaneous symmetry breaking pattern is not exact, acquiring a finite mass $M_\pi^2 = c/f_\pi$.

IV. THE FUNCTIONAL RENORMALIZATION GROUP

In this section, we provide a brief introduction to the FRG, following the interpretation provided by Wetterich *et al.* [51–54], see [39–43] for reviews. When performing an FRG study, one changes the focus from the usual generating functional of the theory, or the partition function, to the effective action $\Gamma[\Phi]$, which serves as the generating functional of 1PI vertex functions. Within the FRG formalism, similarly to Wilson's approach to renormalization, for the computation of $\Gamma[\Phi]$ one integrates out the fluctuations by successive momentum shells; this is achieved by introducing the effective average action, $\Gamma_k[\Phi]$, which depends on k that represents the momentum up to which fluctuations have been effectively integrated out, thus serving as a coarse-graining scale. In particular, the effective average action interpolates between the bare classical action, $S_{\text{bare}}[\Phi]$, in the UV, i.e., at the cutoff scale $k = \Lambda$ when no fluctuations have been taken into account,

and the full quantum effective action $\Gamma[\Phi]$ in the IR, i.e., $k = 0$, when all quantum fluctuations have been integrated out, namely

$$\Gamma_{k \rightarrow \infty}[\Phi] = S_{\text{bare}}[\Phi], \quad \Gamma_{k \rightarrow 0}[\Phi] = \Gamma[\Phi]. \quad (16)$$

The evolution of the effective average action from the UV to the IR is described by the FRG flow equation, that is [52,55,56]

$$\partial_k \Gamma_k[\Phi] = \text{Tr} \left[\left(\frac{1}{2} \partial_k R_k \right) (\Gamma_k^{(2)}[\Phi] + R_k)^{-1} \right] \quad (17)$$

in which the trace is understood as the sum over internal degrees of freedom of the theory, such as color, flavor, spin etc, as well as an integral over Fourier momenta. R_k in Eq. (17) is a regulator which effectively defines the support of the momentum integral in the UV and acts as a screening term in the IR. R_k must be chosen in order for Γ_k to fulfill the conditions (16). In particular, in order to recover the full quantum effective action in the IR, it has to vanish for $k \rightarrow 0$. Moreover, R_k has to diverge for large k in order to ensure that the bare action represents a stationary point for the path integral through which Γ_k is introduced.

$G_k[\Phi] \equiv (\Gamma_k^{(2)}[\Phi] + R_k)^{-1}$ in Eq. (17) indicates the exact, scale dependent propagator, thus the FRG flow equation has a one-loop structure. Despite this apparent simplicity, it still consists of a hard-to-solve functional integro-differential equation; hence, except for very special cases (see for example [57–59]), one has to rely on approximations in order to solve it. A first possibility is called the vertex-expansion [53,60], in which $\Gamma_k[\Phi]$ is expanded in powers of the fields Φ around a certain field configuration Φ_0 , and the expansion coefficients are the vertex functions $\Gamma_k^{(n)}(x_1, \dots, x_n) = \delta^n \Gamma_k[\Phi] / \delta \Phi(x_1) \cdots \delta \Phi(x_n) |_{\Phi=\Phi_0}$. Plugging the vertex expansion into the FRG flow equation, one obtains a system of infinite coupled integro-differential equations which are then truncated at certain finite order.

Another approximation scheme, which is the one we adopt in the present work, is called the derivative expansion [43,62], which approximates $\Gamma_k[\Phi]$ in terms of powers of space-time derivatives of the fields. Also in this case one would obtain an infinite system of coupled equations, one per each operator compatible with the symmetries of the theory, and thus for a practical solution one has to choose an order of space-time derivatives of the fields to which the action is truncated. One of the main advantages of the derivative expansion is that one does not need to assume an analytic behavior in field space of the effective action during the flow evolution, which on the other hand is required by the vertex expansion.

In this work, we focus on critical phenomena which involve second order phase transitions (in the chiral limit), crossovers and critical endpoints in the phase diagram. It is known that, under these conditions, the free energy is not

arbitrarily differentiable (see for example [41,94–96]); furthermore, the effective action can develop discontinuities, or in general singular points, when dealing with such a kind of phenomena [97–100]. This suggests us to take advantage of the properties of the derivative expansion, also at the lowest order called local potential approximation (LPA) [100]. Particularly, we adopt the LPA ansatz for the QM model at finite temperature and quark number density

$$\Gamma_k[\bar{\Psi}, \Psi, \phi] = \int_0^{1/T} dx_4 \int d^3x \left\{ \bar{\psi}(\gamma_\mu \partial^\mu + h(\sigma + i\gamma^5 \vec{\tau} \vec{\pi}) - \mu\gamma_0)\psi + \frac{1}{2}(\partial_\mu \sigma)^2 + \frac{1}{2}(\partial_\mu \vec{\pi})^2 + U_k(\sigma^2 + \vec{\pi}^2) - c\sigma \right\}. \quad (18)$$

Using the three-dimensional Litim regulator [101,102] for both fermions and bosons,

$$R_{k,B}(p) = (k^2 - p^2)\Theta(k^2 - p^2) \quad (19)$$

$$R_{k,F}(p) = i\not{p} \left(\sqrt{\frac{k^2}{p^2} - 1} \right) \Theta(k^2 - p^2), \quad (20)$$

we get the flow equation for the effective potential, that is

$$\partial_t U_k(\sigma) = -\frac{k^5}{12\pi^2} \left\{ \left[\frac{1}{E_{k,\sigma}} \coth\left(\frac{E_{k,\sigma}}{2T}\right) + \frac{3}{E_{k,\pi}} \coth\left(\frac{E_{k,\pi}}{2T}\right) \right] - 4N_c \frac{1}{E_\psi} \left[\tanh\left(\frac{E_\psi - \mu}{2T}\right) + \tanh\left(\frac{E_\psi + \mu}{2T}\right) \right] \right\}, \quad (21)$$

with $t = -\ln k/\Lambda$ and

$$E_{k,\sigma} = \sqrt{k^2 + \partial_\sigma^2 U_k(\sigma)}, \quad E_{k,\pi} = \sqrt{k^2 + \frac{\partial_\sigma U_k(\sigma)}{\sigma}}. \quad (22)$$

Moreover,

$$E_\psi = \sqrt{p^2 + M^2}, \quad (23)$$

with $M = h\langle\sigma\rangle$ denoting the previously defined constituent quark mass.

Analogously to, e.g., [100,103,104], we introduce the following variables

$$u_k(\sigma) = \partial_\sigma U_k(\sigma), \quad u'_k(\sigma) = \partial_\sigma u_k(\sigma). \quad (24)$$

Taking the derivative of Eq. (21) with respect to σ we are able to cast the FRG flow equation into an advection-diffusion equation with a source term [98,99], thus obtaining

$$\partial_t u_k(\sigma) + \partial_\sigma f_k(\sigma, u_k(\sigma)) = \partial_\sigma g_k(u'_k(\sigma)) + N_c \partial_\sigma S_k(\sigma) \quad (25)$$

where we defined the advection flux as

$$f_k(\sigma, u_k(\sigma)) = \frac{k^5}{4\pi^2} \frac{1}{E_{k,\pi}} \coth\left(\frac{E_{k,\pi}}{2T}\right), \quad (26)$$

the diffusion flux, namely

$$g_k(u'_k(\sigma)) = -\frac{k^5}{12\pi^2} \frac{1}{E_{k,\sigma}} \coth\left(\frac{E_{k,\sigma}}{2T}\right), \quad (27)$$

and finally the source term

$$N_c S_k(\sigma) = \frac{N_c k^5}{3\pi^2} \frac{1}{E_\psi} \left[\tanh\left(\frac{E_\psi - \mu}{2T}\right) + \tanh\left(\frac{E_\psi + \mu}{2T}\right) \right]. \quad (28)$$

In this framework, the derivative of the potential $u_k(\sigma)$ plays the role of a conserved quantity, in the sense that it satisfies a generalized conservation law [57,97,105]. Each of the previously defined contributions arises from the various particle species involved in the model. The advection flux, which is responsible of the bulk motion of the conserved quantity u , is originated from the pions. Indeed, there is a factor 3 that appears in Eq. (21) and multiplying the advection term. Furthermore, as it can be seen from the definition of the energy $E_{k,\pi}$, the mass term for the pions, $u_k(\sigma)/\sigma$, vanishes at the minimum of the effective potential, in agreement with the nature of the pions as Goldstone bosons (since the explicit symmetry breaking term is linear in the sigma field, it does not contribute to the flow equation and is just added to the IR potential). One can verify that the speed of characteristics $\partial_u f_k(\sigma, u_k(\sigma))$ is positive if $\sigma < 0$ and negative if $\sigma > 0$, implying that the conserved quantity $u_k(\sigma)$ and the minimum of the potential are always transported toward smaller values of σ by the advection.

On the other hand, the one radial sigma mode produces the diffusion term, which depends on the curvature mass $u'_k(\sigma)$. The diffusion has no specific direction since it depends on the local gradients of the conserved quantity, meaning that smears out peaks and discontinuities.

The fermionic loop gives rise to a time and σ dependent source term, which we identify as such since it is independent of the conserved quantity $u_k(\sigma)$.

In order to compute thermodynamic quantities we need the effective potential, but solving the flow equation (25) we obtain its derivative with respect to σ . This means that we need to integrate the solution in σ , and so the effective potential would be defined up to an arbitrary integration constant, which is σ -independent but in principle T and μ -dependent. Thus to obtain the correct thermodynamic properties we need to calculate this constant using directly

the flow equation (21), evaluated in a generic point (that for us is $\sigma = 0$). Thus, together with Eq. (25) we also solve

$$\partial_t U_k(0) = -\frac{k^5}{12\pi^2} \left\{ \left[\frac{4}{E_{k,\sigma}(\sigma=0)} \coth\left(\frac{E_{k,\sigma}(\sigma=0)}{2T}\right) \right] - 4N_c \frac{1}{k} \left[\tanh\left(\frac{k-\mu}{2T}\right) + \tanh\left(\frac{k+\mu}{2T}\right) \right] \right\}.$$

V. RESULTS

Throughout this section we compare the results obtained within the mean field approximation, obtained by neglecting the bosonic fluctuations, with the calculation that takes into account the fluctuations by solving the full FRG flow equation for the average effective action. In the mean field approximation we first introduce the rescaling $\sigma \rightarrow \sqrt{N_c}\sigma$, $U_k(\sigma) \rightarrow N_c U_k(\sigma)$ and $u_k(\sigma) \rightarrow \sqrt{N_c}u_k(\sigma)$, then we get the rescaled flow equation

$$\begin{aligned} \partial_t u_k(\sigma) + \frac{1}{\sqrt{N_c}} \partial_{u_k} f_k(\sigma, u_k(\sigma)) u_k'(\sigma) \\ = \frac{1}{\sqrt{N_c}} \partial_\sigma g_k(u_k'(\sigma)) + \partial_\sigma S_k(\sigma). \end{aligned} \quad (29)$$

The mean field flow equation is obtained in the $N_c \rightarrow \infty$ limit, that is

$$\partial_t u_k(\sigma) = \partial_\sigma S_k(\sigma). \quad (30)$$

As initial condition in the UV ($k = \Lambda$ or $t = 0$) for the flow equation we choose a quartic potential

$$U_\Lambda(\sigma) = \frac{m_{\text{UV}}^2}{2} \sigma^2 + \frac{\lambda_{\text{UV}}}{4} \sigma^4. \quad (31)$$

Due to the presence of a finite cutoff Λ , when performing the Matsubara sum, thermal modes with $2\pi T > \Lambda$ are factually excluded. This is a serious problem especially for the calculation of thermodynamic quantities at high temperatures. This issue can be fixed including the missing high-momentum modes in the effective potential. Since one expects the fermionic degrees of freedom to be relevant at higher temperature, a standard procedure consists of integrating the fermionic part of Eq. (21) from $k \rightarrow \infty$ to $k = \Lambda$ and add it to the effective potential. So we calculate

$$U_\Lambda^\infty(\sigma) = \int_\infty^\Lambda S_k(\sigma) dk \quad (32)$$

and then add it to the effective potential at the UV scale Λ

$$U_\Lambda(\sigma) \rightarrow U_\Lambda(\sigma) + U_\Lambda^\infty(\sigma) \quad (33)$$

Our set of parameters is $\Lambda = 1.0 \text{ GeV}$, $f_\pi = 0.093 \text{ GeV}$, $h = 3.6$, $c = 1.78 \times 10^{-3} \text{ GeV}^3$. The initial condition

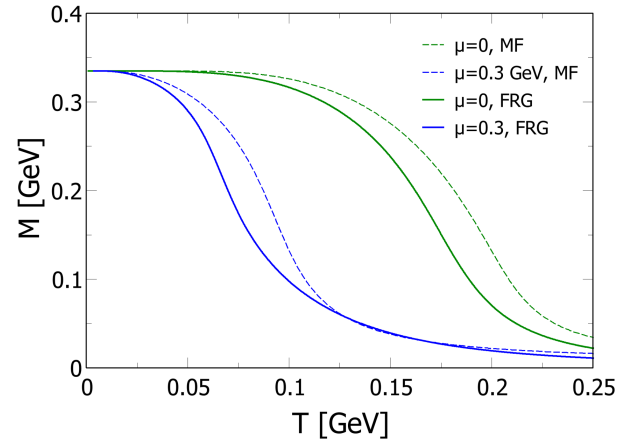


FIG. 2. Constituent quark mass, $M = h\langle\sigma\rangle$, versus temperature, for $\mu = 0$ and $\mu = 0.3 \text{ GeV}$. MF and FRG stand for mean field and functional renormalization group respectively.

parameters are $m_{\text{UV}} = 0.762 \text{ GeV}$ and $\lambda_{\text{UV}} = 1.05$ for MF calculations, and $m_{\text{UV}} = 0.812 \text{ GeV}$ and $\lambda_{\text{UV}} = 3.08$ in the FRG case. These parameters are chosen such that in the vacuum we get $\langle\sigma\rangle = f_\pi$ and $\partial_{\sigma\sigma}^2 U(\langle\sigma\rangle) = M_\sigma^2 = 0.36 \text{ GeV}^2$.

In Fig. 2 we show the constituent quark mass, $M = h\langle\sigma\rangle$, versus temperature, for $\mu = 0$ and $\mu = 0.3 \text{ GeV}$; $\langle\sigma\rangle$ corresponds to the value of σ that minimizes the effective action. We note that there is a range of temperatures in which the condensate decreases from its zero temperature value to a smaller one, signaling the crossover from the low temperature phase in which chiral symmetry is spontaneously broken to the high temperature phase in which the symmetry is (approximately) restored. The picture remains qualitatively the same also after fluctuations are included; quantitatively, fluctuations lower the temperature range in which the chiral crossover takes place. We also note that increasing the chemical potential results in the hardening of the crossover, since changes in $\langle\sigma\rangle$ occur in a smaller range of temperature.

The results shown in Fig. 2 allow us to define a (pseudo) critical temperature, T_c , as the temperature at which the highest change of $\langle\sigma\rangle$ occurs. In Fig. 3 we plot T_c versus μ for both the mean field case and the full FRG calculation. Below the critical lines the chiral symmetry is spontaneously broken, while above the lines chiral symmetry is approximately restored. For both cases the lines are stopped at the critical endpoint, where the crossover changes into a real second order phase transition where the chiral susceptibility diverges; for larger values of μ the phase transition is of the first order: in this case the effective potential exhibits two separate finite minima which become degenerate at the phase transition.

Next we turn to the main focus of this work, namely the thermodynamic geometry. First, we show in Fig. 4 the determinant of the thermodynamic metric, g , versus μ , computed at $T = T_c$. We present the results obtained within

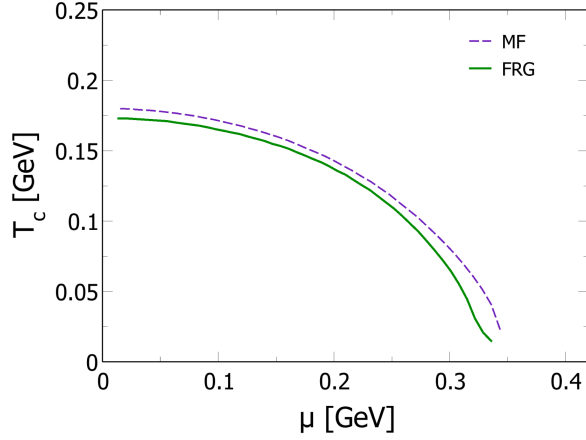


FIG. 3. Critical temperature, T_c , versus μ , for the mean field (dashed line) and the full FRG (solid line) calculations.

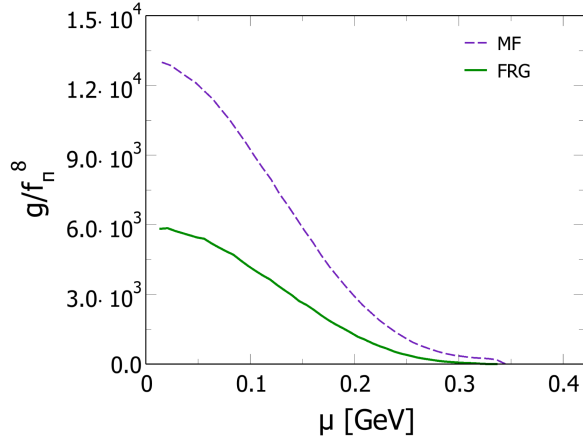


FIG. 4. Determinant of the thermodynamic metric, g , versus μ computed at $T = T_c$, within the mean field approximation (dashed line) and FRG (solid line).

the mean field approximation and within the FRG. The results are in qualitative agreement with [28], where fluctuations were introduced within a gaussian approximation. $g = 0$ corresponds to the thermodynamic instability of the system, that is to a phase transition. We do not find $g = 0$ because in this model chiral symmetry is explicitly, albeit softly, broken by the finite quark mass, hence a phase transition is replaced by a smooth crossover. However, $g(T_c)$ decreases with μ , signaling that the system is approaching criticality, that is the critical endpoint. Moreover, we note that including fluctuations results in the lowering of g , in agreement with previous findings [28].

We now discuss the thermodynamic curvature, R . It is expected that R diverges at a second order phase transition, while it is not obvious the behavior of R near a smooth crossover. In order to better understand the results on R obtained within the FRG, we preliminarily analyze the curvature versus T at $\mu = 0$, with and without fluctuations, for several values of the parameter c that regulates the

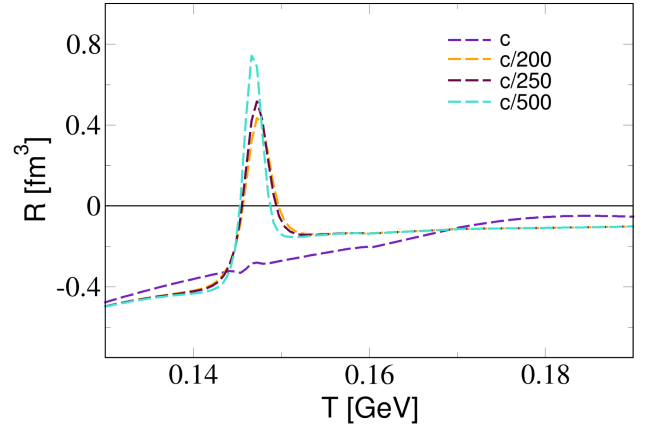
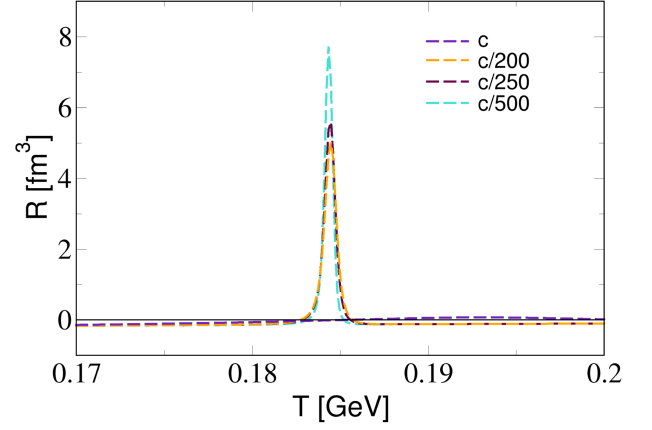


FIG. 5. Thermodynamic curvature, R , versus T , for several values of c . Upper panel corresponds to the mean field approximation, while the lower panel to the calculations within the FRG. $c = M_\pi^2 f_\pi$ denotes the physical value of the symmetry breaking parameter in Eq. (14).

explicit breaking of chiral symmetry. In fact, in the limit $c = 0$, chiral symmetry is not explicitly broken and restoration of chiral symmetry at $\mu = 0$ happens by a second order phase transition. Performing calculations of R in the chiral limit is numerically demanding near the phase transition, hence we limit ourselves to analyze cases in which c is small but nonzero. In order to avoid confusion, from now on with c we denote solely the value of the parameter at the physical point, namely $c = M_\pi^2 f_\pi$; we then artificially lower the value of this parameter.

In Fig. 5, we plot R versus T at $\mu = 0$ within the mean field approximation (upper panel) and with fluctuations included (lower panel); we show results for several values of the symmetry breaking parameter in Eq. (14), namely the physical value, then $c/200$, $c/250$ and $c/500$. We note in both panels of Fig. 5 that as the chiral limit is approached, the curvature is enhanced in the pseudocritical region, while the peak of R becomes smoother as c approaches the one in the physical limit. Moreover, including fluctuations results in the lowering of the peaks of R in the pseudocritical region. Within the mean field approximation, R changes sign around T_c , in agreement with previous

results [27,28,38]: this was interpreted as the emergence of a bosonlike behavior of the system around T_c , namely of a statistical attraction in phase space due to long range correlations that develop around T_c that overcomes the statistical fermionic repulsion. This behavior of R is also found when fluctuations are included (lower panel of Fig. 5). However, we note that fluctuations lower the overall magnitude of R , in agreement with [28]. We also note that the peaks of R become more prominent as the chiral limit is approached, and changes its sign, as in the mean field calculations. Hence, it is likely that the qualitative behavior of R is independent on the approximation used (mean field versus FRG), at the physical point, and so does the change of nature from fermionlike to bosonlike in proximity of the crossover. The results shown in Fig. 5 will be useful to interpret the behavior of R we discuss below. As a final remark, we note that the peak of R moves toward smaller temperatures as the chiral limit is approached. This is in agreement with the fact that the critical temperature is lower in the chiral limit. We will see that as the critical point is approached, the change of sign of R appears both in the mean field and in the FRG cases.

In Fig. 6 we plot R versus T for several values of μ , obtained within the mean field approximation and the full FRG calculation at the physical point $c = M_{\pi}^2 f_{\pi}$. In both the MF and FRG panels of Fig. 6, we multiplied the results by 100 in all but the $\mu = 0.3$ GeV cases to make the results more readable. Firstly, we note that the trend of R is qualitatively similar in both calculations. Within the mean field approximation, at $\mu = 0$ the curvature locally develops a peak in correspondence of the chiral crossover, signaling that R is capable to capture the pseudocritical behavior of the quark condensate. Increasing the chemical potential, R maintains its local peak structure, but as the critical endpoint is approached, the peaks become more pronounced. This is in agreement with the general understanding on R which is expected to diverge at a second order phase transition. Moreover, we note that at large μ the thermodynamic curvature develops several peaks in the temperature range of the chiral crossover, although the most pronounced peak does not necessarily show up at the critical temperature. This behavior, already noticed in [27], shows that R is not necessarily as sensitive as other quantities, like the chiral susceptibility or $|dM/dT|$, at the changes of the quark condensate at $T = T_c$, but it is still capable to measure sensible deviations in the pressure around the chiral crossover.

Including fluctuations does not change the qualitative behavior of R . Therefore, we conclude that the fact that R is sensitive to the chiral crossover is not an artifact of the mean field approximation, rather it is a quite solid statement. However, as already remarked in Fig. 5, the inclusion of fluctuations lowers the value of R around the chiral crossover; particularly, when μ is small, R remains negative also around the crossover, while in the mean field

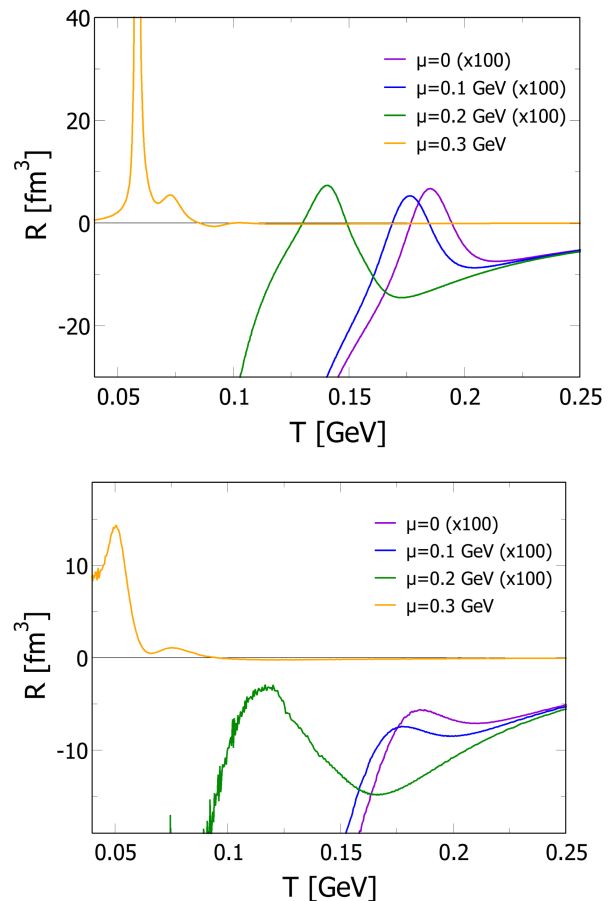


FIG. 6. Thermodynamic curvature, R , versus T , for several values of μ . Calculations correspond to the mean field approximation (upper panel) and the FRG scheme (lower panel).

approximation it changes sign. Therefore, it is likely that the change of nature of the interaction at the mesoscopic level, from fermionlike to bosonlike, depends on the approximation used in the calculation when the system is far from criticality. Hence, this implies that, at small μ , the fluctuations substantially change the geometry of the manifold.

On the other hand, when the critical endpoint is approached at large μ , we find that R changes sign also in the FRG calculation, and the mean field results do not qualitatively differ from the those obtained within the FRG. Hence, we conclude that when this system approaches criticality, R changes sign and locally develops a marked peak: this conclusion was anticipated in previous mean field calculations [27,38] and stands also in case fluctuations are taken into account via FRG.

VI. CONCLUSIONS AND OUTLOOK

We studied the thermodynamic geometry, and in particular computed the thermodynamic curvature R , of the chiral phase transition of quantum chromodynamics, within the quark-meson model and the functional renormalization

group method. The advantage of this method is that it allows to exactly include fluctuations, differently from previous approaches [28] in which fluctuations were introduced only within a Gaussian approximation. As a matter of fact, the inclusion of quantum fluctuations via the functional renormalization group represents a remarkable improvement compared to previous mean field calculations. We found that the qualitative behavior of R is not very different from the one previously computed within mean field calculations, as well as within calculation schemes that include fluctuations by a Gaussian approximation. In particular, R seems to keep its local peak structure in proximity of the chiral crossover at small chemical potential; moreover, it is enhanced at the critical point, signaling that when the system approaches criticality R could diverge, supporting the arguments of hyperscaling [1].

We also found that the change of sign of R near the chiral crossover, discussed previously in the literature [27,28,38,90,91], also happens when fluctuations are taken into account within the functional renormalization group approach; furthermore, as the system approaches criticality, the change of sign from negative (fermionlike behavior) to positive (bosonlike behavior) takes also place. Hence, we conclude that the change of sign of R near the critical endpoint seems to be quite a robust prediction of the chiral effective models.

It will be interesting to analyze if the behavior of R we highlighted in this article does not change when the truncation adopted in the functional renormalization group

approach is improved; for example, the inclusion of the scale-dependent wave function renormalization factors of the boson and the quark fields is worth of further investigation, due to the possible link of this to the formation of inhomogeneous phases at large chemical potential. Another possible improvement is the introduction of other condensation channels, which could include diquarks or meson condensates. A potential application would be the QM model with a finite isospin chemical potential, μ_I , at vanishing (or small) μ . This would be extremely interesting, due to the opportunity to directly compare the obtained results with lattice QCD calculations, since a finite μ_I does not lead to a sign problem, and would give the opportunity to study R in presence of potentially two condensates, namely a pion condensate beside the chiral condensate. We plan to address these issues in the near future.

ACKNOWLEDGMENTS

M. R. acknowledges John Petrucci for inspiration. M. R. and F. M. acknowledges Gabriele Parisi for numerous discussions. F. M. acknowledges discussions with D. Rischke. This work has been partly funded by the European Union—Next Generation EU through the research Grant No. P2022Z4P4B “SOPHYA—Sustainable Optimised Physics Algorithms: Fundamental physics to build an advanced society” under the Program No. PRIN 2022 PNRR of the Italian Ministero dell’Università e Ricerca (MUR).

-
- [1] G. Ruppeiner, Thermodynamics: A Riemannian geometric model, *Phys. Rev. A* **20**, 1608 (1979).
 - [2] G. Ruppeiner, Application of Riemannian geometry to the thermodynamics of a simple fluctuating magnetic system, *Phys. Rev. A* **24**, 488 (1981).
 - [3] G. Ruppeiner, New thermodynamic fluctuation theory using path integrals, *Phys. Rev. A* **27**, 1116 (1983).
 - [4] G. Ruppeiner, Thermodynamic critical fluctuation theory?, *Phys. Rev. Lett.* **50**, 287 (1983).
 - [5] G. Ruppeiner, Thermodynamics near the correlation volume, *Phys. Rev. A* **31**, 2688 (1985).
 - [6] G. Ruppeiner, Comment on “Length and curvature in the geometry of thermodynamics”, *Phys. Rev. A* **32**, 3141 (1985).
 - [7] G. Ruppeiner, Thermodynamics at less than the correlation volume, *Phys. Rev. A* **34**, 4316 (1986).
 - [8] G. Ruppeiner and C. Davis, Thermodynamic curvature of the multicomponent ideal gas, *Phys. Rev. A* **41**, 2200 (1990).
 - [9] G. Ruppeiner and J. Chance, Thermodynamic curvature of a one-dimensional fluid, *J. Chem. Phys.* **92**, 3700 (1990).
 - [10] G. Ruppeiner, Riemannian geometric theory of critical phenomena, *Phys. Rev. A* **44**, 3583 (1991).
 - [11] G. Ruppeiner, Asymmetric free energy from Riemannian geometry, *Phys. Rev. E* **47**, 934 (1993).
 - [12] G. Ruppeiner, Riemannian geometry in thermodynamic fluctuation theory, *Rev. Mod. Phys.* **67**, 605 (1995); **68**, 313(E) (1996).
 - [13] G. Ruppeiner, Riemannian geometric approach to critical points: General theory, *Phys. Rev. E* **57**, 5135 (1998).
 - [14] G. Ruppeiner, Riemannian geometry of thermodynamics and systems with repulsive power-law interactions, *Phys. Rev. E* **72**, 016120 (2005).
 - [15] G. Ruppeiner, Thermodynamic curvature measures interactions, *Am. J. Phys.* **78**, 1170 (2010).
 - [16] G. Ruppeiner, Thermodynamic curvature and phase transitions in Kerr-Newman black holes, *Phys. Rev. D* **78**, 024016 (2008).
 - [17] G. Ruppeiner, A. Sahay, T. Sarkar, and G. Sengupta, Thermodynamic geometry, phase transitions, and the widom line, *Phys. Rev. E* **86**, 052103 (2012).
 - [18] G. Ruppeiner, Thermodynamic curvature: Pure fluids to black holes, *J. Phys. Conf. Ser.* **410**, 012138 (2013).

- [19] G. Ruppeiner, Thermodynamic curvature from the critical point to the triple point, *Phys. Rev. E* **86**, 021130 (2012).
- [20] H.-O. May, P. Mausbach, and G. Ruppeiner, Thermodynamic curvature for attractive and repulsive intermolecular forces, *Phys. Rev. E* **88**, 032123 (2013).
- [21] G. Ruppeiner, Thermodynamic curvature and black holes, *Springer Proc. Phys.* **153**, 179 (2014).
- [22] G. Ruppeiner, Unitary thermodynamics from thermodynamic geometry, *J. Low Temp. Phys.* **174**, 13 (2014).
- [23] G. Ruppeiner and S. Bellucci, Thermodynamic curvature for a two-parameter spin model with frustration, *Phys. Rev. E* **91**, 012116 (2015).
- [24] H.-O. May, P. Mausbach, and G. Ruppeiner, Thermodynamic geometry of supercooled water, *Phys. Rev. E* **91**, 032141 (2015).
- [25] G. Ruppeiner, Some early ideas on the metric geometry of thermodynamics, *J. Low Temp. Phys.* **185**, 246 (2016).
- [26] G. Ruppeiner, N. Dyjack, A. McAloon, and J. Stoops, Solid-like features in dense vapors near the fluid critical point, *J. Chem. Phys.* **146**, 224501 (2017).
- [27] B. Zhang, S.-S. Wan, and M. Ruggieri, Thermodynamic geometry of the quark-meson model, *Phys. Rev. D* **101**, 016014 (2020).
- [28] P. Castorina, D. Lanteri, and M. Ruggieri, Fluctuations and thermodynamic geometry of the chiral phase transition, *Phys. Rev. D* **102**, 116022 (2020).
- [29] M. Gell-Mann and M. Levy, The axial vector current in beta decay, *Nuovo Cimento* **16**, 705 (1960).
- [30] V. Koch, Aspects of chiral symmetry, *Int. J. Mod. Phys. E* **06**, 203 (1997).
- [31] M. E. Peskin and D. V. Schroeder, *An Introduction to Quantum Field Theory* (Westview Press, Addison-Wesley, Reading, USA, 1995), p. 842.
- [32] S. Weinberg, *The Quantum Theory of Fields* (Cambridge University Press, Cambridge, England, 1996), Vol. 2.
- [33] M. Cheng, S. Ejiri, P. Hegde, F. Karsch, O. Kaczmarek, E. Laermann, R. D. Mawhinney, C. Miao, S. Mukherjee, P. Petreczky, C. Schmidt, and W. Soeldner, Equation of state for physical quark masses, *Phys. Rev. D* **81**, 054504 (2010).
- [34] A. Bazavov *et al.* (HotQCD Collaboration), Chiral and deconfinement aspects of the QCD transition, *Phys. Rev. D* **85**, 054503 (2012).
- [35] S. Borsanyi, G. Endrodi, Z. Fodor, A. Jakovac, S. D. Katz, S. Krieg, C. Ratti, and K. K. Szabo, The QCD equation of state with dynamical quarks, *J. High Energy Phys.* **11** (2010) 077.
- [36] K. Fukushima and T. Hatsuda, The phase diagram of dense QCD, *Rep. Prog. Phys.* **74**, 014001 (2010).
- [37] A. Bzdak, S. Esumi, V. Koch, J. Liao, M. Stephanov, and N. Xu, Mapping the phases of quantum chromodynamics with beam energy scan, *Phys. Rep.* **853**, 1 (2020).
- [38] P. Castorina, D. Lanteri, and S. Mancani, Thermodynamic geometry of Nambu–Jona Lasinio model, *Eur. Phys. J. Plus* **135**, 43 (2020).
- [39] J. M. Pawłowski, Aspects of the functional renormalisation group, *Ann. Phys. (Amsterdam)* **322**, 2831 (2007).
- [40] H. Gies, Introduction to the functional RG and applications to gauge theories, *Lect. Notes Phys.* **852**, 287 (2012).
- [41] P. Kopietz, L. Bartosch, and F. Schütz, *Introduction to the Functional Renormalization Group* (Springer, Berlin, Heidelberg, 2010), Vol. 798.
- [42] N. Dupuis, L. Canet, A. Eichhorn, W. Metzner, J. M. Pawłowski, M. Tissier, and N. Wschebor, The nonperturbative functional renormalization group and its applications, *Phys. Rep.* **910**, 1 (2021).
- [43] J. Berges, N. Tetradis, and C. Wetterich, Nonperturbative renormalization flow in quantum field theory and statistical physics, *Phys. Rep.* **363**, 223 (2002).
- [44] K. G. Wilson, Renormalization group and critical phenomena. 2. Phase space cell analysis of critical behavior, *Phys. Rev. B* **4**, 3184 (1971).
- [45] K. G. Wilson, Renormalization group and critical phenomena. 1. Renormalization group and the Kadanoff scaling picture, *Phys. Rev. B* **4**, 3174 (1971).
- [46] K. G. Wilson and J. Kogut, The renormalization group and the ϵ expansion, *Phys. Rep.* **12**, 75 (1974).
- [47] K. G. Wilson, The renormalization group: Critical phenomena and the Kondo problem, *Rev. Mod. Phys.* **47**, 773 (1975).
- [48] K. G. Wilson, Problems in physics with many scales of length, *Sci. Am.* **241**, 158 (1979).
- [49] J. Polchinski, Renormalization and effective Lagrangians, *Nucl. Phys.* **B231**, 269 (1984).
- [50] A. Hasenfratz and P. Hasenfratz, Renormalization group study of scalar field theories, *Nucl. Phys.* **B270**, 687 (1986).
- [51] U. Ellwanger, FLOW equations for N point functions and bound states, *Z. Phys. C* **62**, 503 (1994).
- [52] C. Wetterich, Exact evolution equation for the effective potential, *Phys. Lett. B* **301**, 90 (1993).
- [53] T. R. Morris, On truncations of the exact renormalization group, *Phys. Lett. B* **334**, 355 (1994).
- [54] M. Reuter and C. Wetterich, Effective average action for gauge theories and exact evolution equations, *Nucl. Phys.* **B417**, 181 (1994).
- [55] C. Wetterich, Average action and the renormalization group equations, *Nucl. Phys.* **B352**, 529 (1991).
- [56] T. R. Morris, The exact renormalization group and approximate solutions, *Int. J. Mod. Phys. A* **09**, 2411 (1994).
- [57] A. Koenigstein, M. J. Steil, N. Wink, E. Grossi, J. Braun, M. Buballa, and D. H. Rischke, Numerical fluid dynamics for FRG flow equations: Zero-dimensional QFTs as numerical test cases. I. The O(N) model, *Phys. Rev. D* **106**, 065012 (2022).
- [58] A. Koenigstein, M. J. Steil, N. Wink, E. Grossi, and J. Braun, Numerical fluid dynamics for FRG flow equations: Zero-dimensional QFTs as numerical test cases. II. Entropy production and irreversibility of RG flows, *Phys. Rev. D* **106**, 065013 (2022).
- [59] M. J. Steil and A. Koenigstein, Numerical fluid dynamics for FRG flow equations: Zero-dimensional QFTs as numerical test cases. III. Shock and rarefaction waves in RG flows reveal limitations of the $n \rightarrow \infty$ limit in $o(n)$ -type models, *Phys. Rev. D* **106**, 065014 (2022).

- [60] B. Bergerhoff and C. Wetterich, Effective quark interactions and QCD propagators, *Phys. Rev. D* **57**, 1591 (1998).
- [61] N. Tetradis and D. F. Litim, Analytical solutions of exact renormalization group equations, *Nucl. Phys.* **B464**, 492 (1996).
- [62] J. A. Adams, J. Berges, S. Bornholdt, F. Freire, N. Tetradis, and C. Wetterich, Solving nonperturbative flow equations, *Mod. Phys. Lett. A* **10**, 2367 (1995).
- [63] G. Ruppeiner, Stability and fluctuations in black hole thermodynamics, *Phys. Rev. D* **75**, 024037 (2007).
- [64] H. Janyszek and R. Mrugala, Riemannian geometry and the thermodynamics of model magnetic systems, *Phys. Rev. A* **39**, 6515 (1989).
- [65] H. Janyszek, Riemannian geometry and stability of thermodynamical equilibrium systems, *J. Phys. A* **23**, 477 (1990).
- [66] H. J. R. Mrugala, Riemannian and Finslerian geometry in thermodynamics, *Open Syst. Inf. Dyn.* **1**, 379 (1992).
- [67] H.-O. May and P. Mausbach, Riemannian geometry study of vapor-liquid phase equilibria and supercritical behavior of the lennard-jones fluid, *Phys. Rev. E* **85**, 031201 (2012).
- [68] H.-O. May, P. Mausbach, and G. Ruppeiner, Thermodynamic curvature for attractive and repulsive intermolecular forces, *Phys. Rev. E* **88**, 032123 (2013).
- [69] B. Mirza and H. Mohammadzadeh, Ruppeiner geometry of anyon gas, *Phys. Rev. E* **78**, 021127 (2008).
- [70] H. Oshima, T. Obata, and H. Hara, Riemann scalar curvature of ideal quantum gases obeying gentile's statistics, *J. Phys. A* **32**, 6373 (1999).
- [71] M. R. Ubriaco, Stability and anyonic behavior of systems with m-statistics, *Physica (Amsterdam)* **392A**, 4868 (2013).
- [72] M. R. Ubriaco, The role of curvature in quantum statistical mechanics, *J. Phys. Conf. Ser.* **766**, 012007 (2016).
- [73] H. Mehri-Dehnavi and H. Mohammadzadeh, Thermodynamic geometry of Kaniadakis statistics, *J. Phys. A* **53**, 375009 (2020).
- [74] A. Dey, P. Roy, and T. Sarkar, Information geometry, phase transitions, and the widom line: Magnetic and liquid systems, *Physica (Amsterdam)* **392A**, 6341 (2013).
- [75] G. S. Pankaj Chaturvedi and Anirban Das, Thermodynamic geometry and phase transitions of dyonic charged AdS black holes, *Eur. Phys. J. C* **77**, 110 (2017).
- [76] A. Sahay and R. Jha, Geometry of criticality, supercriticality and Hawking-Page transitions in Gauss-Bonnet-AdS black holes, *Phys. Rev. D* **96**, 126017 (2017).
- [77] T. S. Anurag Sahay and Gautam Sengupta, On the thermodynamic geometry and critical phenomena of AdS black hole, *J. High Energy Phys.* **07** (2010) 082.
- [78] N. P. Jan E. Åman and Ingemar Bengtsson, Geometry of black hole thermodynamics, *Gen. Relativ. Gravit.* **35**, 1733 (2003).
- [79] J. Shen, R.-G. Cai, B. Wang, and R.-K. Su, Thermodynamic geometry and critical behavior of black holes, *Int. J. Mod. Phys. A* **22**, 11 (2007).
- [80] J. E. Aman and N. Pidokrajt, Geometry of higher-dimensional black hole thermodynamics, *Phys. Rev. D* **73**, 024017 (2006).
- [81] T. Sarkar, G. Sengupta, and B. N. Tiwari, Thermodynamic geometry and extremal black holes in string theory, *J. High Energy Phys.* **10** (2008) 076.
- [82] S. Bellucci and B. N. Tiwari, Thermodynamic geometry and topological Einstein–Yang–Mills black holes, *Entropy* **14**, 1045 (2012).
- [83] S.-W. Wei and Y.-X. Liu, Critical phenomena and thermodynamic geometry of charged Gauss-Bonnet AdS black holes, *Phys. Rev. D* **87**, 044014 (2013).
- [84] S.-W. Wei and Y.-X. Liu, Insight into the microscopic structure of an AdS black hole from a thermodynamical phase transition, *Phys. Rev. Lett.* **115**, 111302 (2015); **116**, 169903(E) (2016).
- [85] A. Sahay, Restricted thermodynamic fluctuations and the Ruppeiner geometry of black holes, *Phys. Rev. D* **95**, 064002 (2017).
- [86] G. Ruppeiner, Thermodynamic black holes, *Entropy* **20**, 460 (2018).
- [87] P. K. Yerra and C. Bhamidipati, Ruppeiner geometry, phase transitions and microstructures of black holes in massive gravity, *Int. J. Mod. Phys. A* **35**, 2050120 (2020).
- [88] P. K. Yerra and C. Bhamidipati, Ruppeiner curvature along a renormalization group flow, *Phys. Lett. B* **819**, 136450 (2021).
- [89] D. Lanteri, S.-S. Wan, A. Iorio, and P. Castorina, Stability of Schwarzschild (anti)de Sitter black holes in conformal gravity, *Eur. Phys. J. C* **81**, 576 (2021).
- [90] P. Castorina, M. Imbroschiano, and D. Lanteri, Thermodynamic geometry of strongly interacting matter, *Phys. Rev. D* **98**, 096006 (2018).
- [91] P. Castorina, D. Lanteri, and S. Mancani, Thermodynamic geometry of Nambu–Jona Lasinio model, *Eur. Phys. J. Plus* **135**, 43 (2020).
- [92] L. Diósi, A universal master equation for the gravitational violation of quantum mechanics, *Phys. Lett. A* **120**, 377 (1987).
- [93] L. Diósi, B. Lukács, and A. Rácz, Mapping the van der Waals state space, *J. Chem. Phys.* **91**, 3061 (1989).
- [94] G. Mussardo, *Statistical Field Theory: An Introduction to Exactly Solved Models in Statistical Physics* (Oxford University Press, New York, NY, 2010).
- [95] S. keng Ma, *Modern Theory of Critical Phenomena*, 1st ed. (Imprint Routledge, New York, 2001).
- [96] K. Huang, *Statistical Mechanics*, 2nd ed. (John Wiley & Sons, New York, USA, 1987).
- [97] E. Grossi and N. Wink, Resolving phase transitions with discontinuous Galerkin methods, [arXiv:1903.09503](https://arxiv.org/abs/1903.09503).
- [98] E. Grossi, F. J. Ihssen, J. M. Pawłowski, and N. Wink, Shocks and quark-meson scatterings at large density, *Phys. Rev. D* **104**, 016028 (2021).
- [99] J. Stoll, N. Zorbach, A. Koenigstein, M. J. Steil, and S. Rechenberger, Bosonic fluctuations in the $(1+1)$ -dimensional Gross-Neveu(-Yukawa) model at varying μ and T and finite N , [arXiv:2108.10616](https://arxiv.org/abs/2108.10616).
- [100] F. Murgana, A. Koenigstein, and D. H. Rischke, Reanalysis of critical exponents for the $O(N)$ model via a hydrodynamic approach to the functional renormalization group, *Phys. Rev. D* **108**, 116016 (2023).

- [101] D. F. Litim, Critical exponents from optimized renormalization group flows, *Nucl. Phys.* **B631**, 128 (2002).
- [102] D. F. Litim, Optimized renormalization group flows, *Phys. Rev. D* **64**, 105007 (2001).
- [103] A. Koenigstein, M. J. Steil, N. Wink, E. Grossi, J. Braun, M. Buballa, and D. H. Rischke, Numerical fluid dynamics for FRG flow equations: Zero-dimensional QFTs as numerical test cases—part I: The $O(N)$ model, *Phys. Rev. D* **106**, 065012 (2022).
- [104] E. Grossi and N. Wink, Resolving phase transitions with discontinuous Galerkin methods, *SciPost Phys. Core* **6**, 071 (2023).
- [105] F. Ihssen, F. R. Sattler, and N. Wink, Numerical RG-time integration of the effective potential: Analysis and benchmark, *Phys. Rev. D* **107**, 114009 (2023).